

Spin excitation spectra of the spin-1/2 triangular Heisenberg antiferromagnets from tensor networks

Run-Ze Chi,^{1,2,*} Yang Liu,^{1,2,*} Yuan Wan,^{1,3} Hai-Jun Liao,^{1,3,†} and T. Xiang^{1,2,4,‡}

¹*Beijing National Laboratory for Condensed Matter Physics and Institute of Physics, Chinese Academy of Sciences, Beijing 100190, China.*

²*School of Physical Sciences, University of Chinese Academy of Sciences, Beijing 100049, China.*

³*Songshan Lake Materials Laboratory, Dongguan, Guangdong 523808, China.*

⁴*Beijing Academy of Quantum Information Sciences, Beijing, China.*

Investigation of dynamical excitations is difficult but crucial to the understanding of many exotic quantum phenomena discovered in quantum materials. This is particularly true for highly frustrated quantum antiferromagnets whose dynamical properties deviate strongly from theoretical predictions made based on the spin-wave or other approximations. Here we present a large-scale numerical calculation on the dynamical correlation functions of spin-1/2 triangular Heisenberg model using a state-of-the-art tensor network renormalization group method. The calculated results allow us to gain for the first time a comprehensive picture on the nature of spin excitation spectra in this highly frustrated quantum system. It provides a quantitative account for all the key features of the dynamical spectra disclosed by inelastic neutron scattering measurements for Ba₃CoSb₂O₉, revealing the importance of the interplay between low and high-energy excitations and its renormalization effect to the low-energy magnon bands and high-energy continuums. From the analysis of the projected and sublattice spin structural factors, we further identify the damped longitudinal Higgs modes as well as the hidden magnon band, and predict the spectral functions along three principal axes that can be verified by polarized neutron scattering experiments.

Frustrated quantum magnetism has moved to the forefront of condensed matter physics research. Quite many exotic quantum phenomena driven by the interplay between quantum fluctuations and geometric frustrations, such as quantum spin liquid [1–3], spin fractionalization [4], and magnetic monopoles [5], have been discovered in these systems. The spin-1/2 triangular antiferromagnetic Heisenberg model is a prototypical frustrated magnetic system that has been intensively studied for more than four decades [1, 6–9]. While it is now commonly accepted that its ground state is noncollinear 120° magnetic ordered (Fig. 1.a) [7–9], the physical properties of its excitation states remain elusive.

The linear spin wave theory (LSWT) predicts that there are three magnon excitation modes in the triangular antiferromagnetic Heisenberg model. However, inelastic neutron scattering (INS) measurements on Ba₃CoSb₂O₉ [10–12], which is an excellent realization of the spin-1/2 triangular Heisenberg model [13–16], just observed two branches of magnon excitation modes. More surprisingly, these magnon excitation modes were found to be strongly renormalized around the M point (Fig. 1.b) where the bands bend downward and one of them exhibits a roton-like minimum. Moreover, two strong dispersive continuums of unknown origin are observed above the low-energy magnon bands [11, 12].

A number of theories have been proposed or invoked to explain the exotic magnetic spectra observed in Ba₃CoSb₂O₉, based either on the multi-magnon interac-

tions [10, 12, 17–21] or on the interplay between magnons and fractionalized spinons [22–27]. These theories offered a qualitative explanation to the downward renormalization of the three magnon bands. However, a comprehensive understanding to the dynamical spectra in the whole energy range, especially those in the intermediate- and high-energy scales, is still not available. In particular, it is unknown how the spectral weights are transferred to or from low-energy magnon excitations, damped longitudinal Higgs modes and high-energy continuum. The aim of this work is to resolve these problems through a thorough investigation on the spin-1/2 triangular Heisenberg model using a state-of-the-art tensor-network renormalization group method [28, 29] in combination with the technique of automatic differentiation [30, 31].

Effective Hamiltonian Ba₃CoSb₂O₉ has a highly symmetric hexagonal structure $P6_3/mmc$ [32], and its magnetic Co²⁺ ions with pseudospin-1/2 form a perfect triangular lattice in the ab -plane. It was proposed that this material presents an ideal realization of the paradigmatic spin-1/2 antiferromagnetic Heisenberg model in two dimensions [13–16],

$$H = J \sum_{\langle ij \rangle} (S_i^x S_j^x + S_i^y S_j^y + \Delta S_i^z S_j^z), \quad (1)$$

where $\langle ij \rangle$ runs over all the nearest-neighbor sites of the triangular lattice, J is the antiferromagnetic coupling constant, and Δ is a parameter measuring anisotropy. In our calculation, we adopt the parameters determined from the magnetization, electronic spin resonance, nuclear magnetic resonance and neutron scattering measurements [11–16, 33], namely $J = 1.67$ meV and $\Delta = 0.95$. We ignore the interlayer coupling because it is much

* These authors contributed equally to this work

† navyphysics@iphy.ac.cn

‡ txiang@iphy.ac.cn

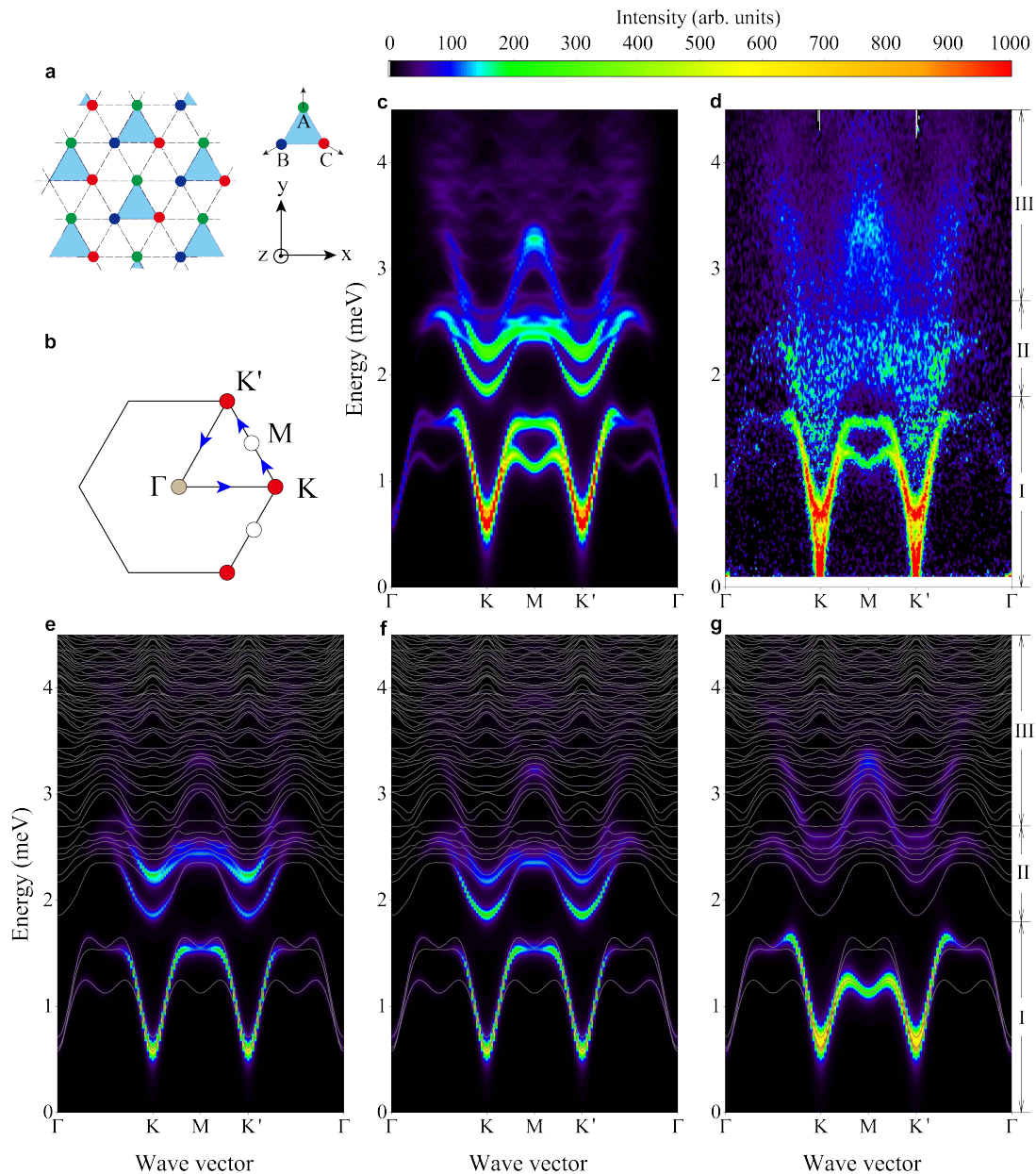


FIG. 1. **Comparison between the tensor-network results and the inelastic neutron scattering (INS) measurement data for the dynamical spin structure factors.** **a:** Trangular lattice and the 120° Néel order in the ground state of the Heisenberg model. The magnetization is ordered along the y -axis direction on sublattice A in the trangular plane. **b:** The first Brillouin zone and the momentum path (the arrowed lines) on which the spectral functions are evaluated. **c:** The total spectral weight of the dynamical spectral function obtained with the tensor-network method for the easy-plane XXZ model with $J = 1.67$ meV and $\Delta = 0.95$. **d:** The INS spectra of $\text{Ba}_3\text{CoSb}_2\text{O}_9$ reproduced using the data published in the Supplementary Materials of Ref. [12]. **e-g:** The spin structure factors along the three principal axes: **e**, $S^{xx}(\mathbf{k}, \omega)$, **f**, $S^{yy}(\mathbf{k}, \omega)$, and **g**, $S^{zz}(\mathbf{k}, \omega)$. Their sum gives the total spectral weight shown in panel **c**. The gray curves shows the energy dispersions of the excitation states. The spectra are divided into three stages according to their dispersions, (I) $0 < E < 1.8$ meV, (II) $1.8 \text{ meV} < E < 2.7$ meV, (III) $E > 2.7$ meV.

smaller than the intralayer coupling [13] and the observed magnetic excitations are almost dispersionless along the c -axis [11].

We employ the tensor-network formalism to simulate the magnetic excitation spectra of $\text{Ba}_3\text{CoSb}_2\text{O}_9$ under the single-mode approximation [34] in the framework of

projected entangled pair states (PEPS). This approximation was first introduced in the framework of matrix product states (MPS) by Ostlund and Rommer in one dimension [35, 36]. It was extended to the PEPS presentation in two dimensions by Vanderstraeten et al [37]. Variational optimizations of local tensors are implemented

with the approach of automatic differentiation first introduced to the tensor-network calculations in Ref. [30]. Recently, this approach was extended to the calculation of excitation states in the single-mode approximation of PEPS [31].

PEPS is a tensor-network factorization of a wave function with an inherent embedding of the entanglement structure of two-dimensional quantum systems. The accuracy of this tensor-network state is controlled by the bond dimension, D , of local tensors. The tensor-network calculation is based on the idea of renormalization group. It does not suffer from the notorious minus-sign problem encountered in the quantum Monte Carlo simulations and is applicable to a strongly correlated system with or without quantum or geometric frustrations, such as the model studied here. Moreover, it obeys the sum rule of spin fluctuation (see Fig. S1 of the Supplementary Material (SM)) and Ref. [31]), and can be directly applied to an infinite-lattice system without being bothered by the finite size effect.

Results Figure 1.c shows the intensity of the spin structural function

$$S(\mathbf{k}, \omega) = \sum_{\alpha} S^{\alpha\alpha}(\mathbf{k}, \omega), \quad (\alpha = x, y, z) \quad (2)$$

$$S^{\alpha\beta}(\mathbf{k}, \omega) = \langle 0 | S_{-\mathbf{k}}^{\alpha} \delta(\omega - H + E_0) S_{\mathbf{k}}^{\beta} | 0 \rangle. \quad (3)$$

calculated using the tensor-network methods along a representative path $\Gamma - K - M - K' - \Gamma$ in the Brillouin zone. Here $S^{\alpha\alpha}(\mathbf{k}, \omega)$ is the dynamical spin-spin correlation function along the three axes. Three striking features are revealed in the spectra in different energy ranges.

In the low energy region, $\omega < 1.8$ meV, two sharp and one weak magnon excitation modes are observed (this can be seen more clearly from Fig. 3). Around the M point, only two sharp excitation modes are visible. The higher energy mode is almost dispersionless, but the lower one exhibits a pronounced roton-like minimum. By carefully examining the energy dispersions, shown by the gray lines in Fig. 1.e, we find that these low-energy spectra are contributed by the three magnon bands, consistent with LSWT. However, the overall energy dispersions of these three magnon excitation modes deviate strongly from the LSWT prediction. The third excitation mode is not clearly seen because the spectral weight of the third band is very small around M. This is consistent with the prediction of a RVB theory [27]. Around the Γ point, the linear magnon dispersions are reproduced, but their intensities are very weak due to the cancellation inside a unit cell. Around the antiferromagnetic vector point K, the spectrum shows a sharp energy dispersion. This dispersion does not go to zero exactly at this point because the long-range correlation of the ground state is terminated by the finite virtual bond dimension of PEPS. Nevertheless, the lowest excitation energy gap at this point, as shown in Fig. S2 of the SM,

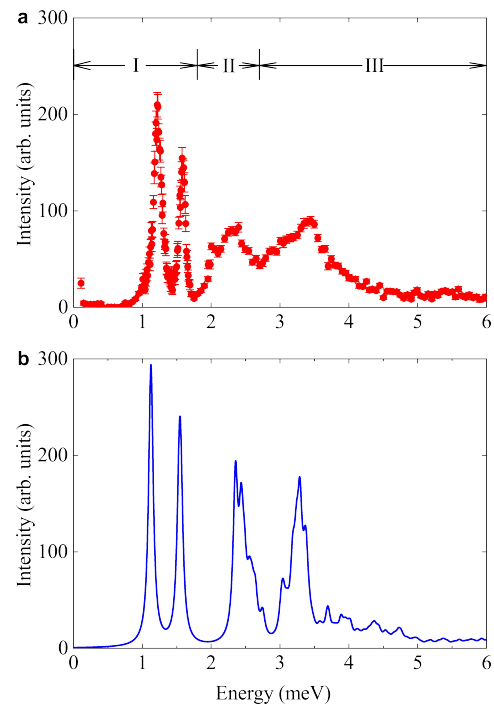


FIG. 2. Comparison of the spectral weight at the M point between the numerical calculation and the INS measurement. **a:** INS intensity for $\text{Ba}_3\text{CoSb}_2\text{O}_9$, reproduced using the data published in Ref. [12]. **b:** Numerical results obtained with the same parameters used as for Fig. 1.

tends to approach zero with the increase of the bond dimension, as a consequence of Goldstone's theorem. In the intermediate energy region, $1.8 \text{ meV} < \omega < 2.7 \text{ meV}$, two W-like excitation modes are observed. These two modes are nearly energy degenerate at the M point, rendering a strong coupling between these two modes. This energy range already falls within the two magnon excitation continuum. In the high energy region, $\omega > 2.7 \text{ meV}$, a weak and smeared W-like dispersive continuum whose tails extend to an energy as high as 6 meV. The energy levels, shown in Fig. 1.e, clearly become more densely packed in this energy range as an indication of excitation continuum. Many of them have invisible spectral weights. The intensity shows a relatively brighter spot at $\omega \sim 3.3 \text{ meV}$ around M.

By comparison with the INS measurement data [11, 12], shown in Fig. 1.d, we find that the numerical result agrees very well with the experimental one, in the whole energy range. This is a surprising result considering that there is not any adjustable parameter used in the calculation. In the high energy region, the INS spectrum looks more diffusive than our numerical result. However, this does not mean that there is no feature in the INS data. In fact, in addition to the two sharp magnon peaks observed in the low-energy region, two more peaks are observed in the high energy spectra of INS at the M point [12]. Fig. 2 compares theoretical result for the energy depen-

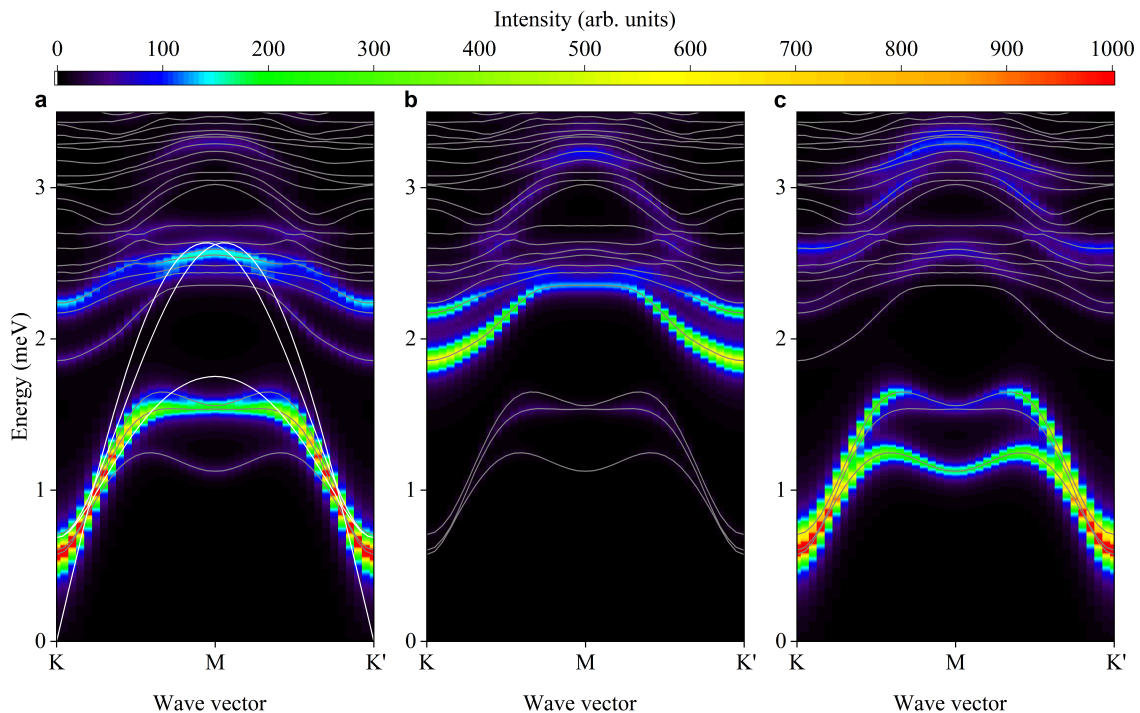


FIG. 3. **Sublattice spectral function in the magnetic Brillouin zone.** The momentum runs along the primary vectors of the magnetic Brillouin zone that is equivalent to the path $K - M - K'$ in the original Brillouin zone. The longitudinal direction is defined along the direction of the magnetization of sublattice A, i.e. along the y -axis. **a:** In-plane transverse fluctuation modes. **b:** Longitudinal fluctuation modes. **c:** Out-of-plane transverse fluctuation modes. The energy dispersions of magnons predicted by LSWT (white curves) are also shown in panel **a** for comparison.

dence of the intensity with the experimental one at that point [12]. Again, the four peak spectrum with the peak energies obtained from the numerical calculation agree well with the experimental ones. This is the first time the two broad spectral peaks above 2 meV are disclosed in a theoretical calculation. The two high-energy INS peaks are broader than the numerical ones. This is the reason why the high-energy spectrum of INS looks more diffusive than the numerical result. It may result from the finite bond dimension effect in the tensor-network calculation. This effect reduces the correlation lengths of low-lying excitations, leading to an underestimation of the interaction between the high-energy excitation modes and low-energy magnons.

The projected spectra functions along the three principal axes, $S^{xx}(\mathbf{k}, \omega)$, $S^{yy}(\mathbf{k}, \omega)$ and $S^{zz}(\mathbf{k}, \omega)$, can be measured by utilizing spin polarized neutrons. This provides a unique approach to experimentally test our numerical predictions shown in Fig. 1.e-g. As the magnetization is co-planar ordered, the low energy spectral weight of $S^{zz}(\mathbf{k}, \omega)$ contributes mainly from the out-of-plane transverse fluctuations. The low-energy spectral weights of $S^{xx}(\mathbf{k}, \omega)$ and $S^{yy}(\mathbf{k}, \omega)$, on the other hand, contribute from the in-plane transverse as well as longitudinal fluctuations.

To further elucidate the microscopic nature of low energy excitations, we investigate the sublattice spectral

functions in the framework of coordinates where all magnetic ordered spins are locally rotated towards the positive direction of the y -axis. We denote the corresponding spectral functions as $\tilde{S}^{xx}(\mathbf{k}, \omega)$, $\tilde{S}^{yy}(\mathbf{k}, \omega)$ and $\tilde{S}^{zz}(\mathbf{k}, \omega)$. In this case, $\tilde{S}^{yy}(\mathbf{k}, \omega)$ contributes mainly from the longitudinal fluctuations, $\tilde{S}^{xx}(\mathbf{k}, \omega)$ and $\tilde{S}^{zz}(\mathbf{k}, \omega)$ contribute mainly from the in-plane and out-of-plane transverse fluctuations, respectively.

Figure 3 shows the numerical results for the three sublattice spectral functions (\tilde{S}^{xx} , \tilde{S}^{yy} , \tilde{S}^{zz}). Compared with the LSWT prediction (Fig. 3.a), we find that the three magnon bands are strongly renormalized by their interaction with the high-energy continuum. For the three magnon bands below 1.8 meV, it is clear from Fig. 3.c that the two bands whose energies are largest and smallest at the M point result predominantly from the out-of-plane transverse spin fluctuations. The third magnon band, whose energy lies between the other two bands at the M point, apparently results mainly from the in-plane spin fluctuations.

In the intermediate-energy region, $1.8 < \omega < 2.7$ meV, Fig. 3.b shows clearly the two lowest energy bands contribute mainly by the longitudinal spin fluctuations. This suggests that they are the damped Higgs modes, consistent with the prediction made based on the RVB picture [27]. It can be verified experimentally by taking spin-polarized neutron scattering measurements.

Figure 3 suggests that there is a significant transfer of spectral weights from the three low-energy magnon modes to the high-energy continuum. Such pronounced spectral weight transfer results inevitably from the interaction between the magnon excitations and the high-energy continuum. It leads to the downward bending of the three magnon bands around M, which implies that the interactions of these bands with other excitations around that point are very strong [12, 21, 27]. As the spectral weight of the highest-energy magnon band is almost completely suppressed around the M point in all the directions, it further suggests that the downward bending of this band is not simply a consequence of level repulsion imposed by high-energy excitation states. Otherwise, some remnant spectral weight from the original magnon band should be observed at that point.

Discussion Our tensor network results reveal the key features of the dynamical spin spectra for the spin-1/2 antiferromagnetic Heisenberg model. Not only does it provide a good account for the INS spectrum of $\text{Ba}_3\text{CoSb}_2\text{O}_9$, but also a comprehensive picture for understanding dynamical couplings between different excitation modes without invoking any approximation that is not easy to control. Our result of the sublattice spin structure factors shows unambiguously that the lowest energy band whose intensity is more pronounced around the K point in the intermediate energy region contributes predominately by the longitudinal fluctuations, namely the Higgs modes. The spectral peak around 2.3 meV in Fig. 2.a at the M point, on the other hand, comes mainly from the in-plane transverse excitation mode, but strongly damped by its interaction with the Higgs mode. Furthermore, there are two kinds of transverse excitation modes, from the in-plane and out-of plane spin fluctuations, respectively. Their dynamical responses, as shown in Fig. 1.e-g, can be differentiated by taking INS measurements with polarized neutrons.

This work demonstrates the great potential of the tensor network method in exploring dynamical properties of strongly frustrated antiferromagnets. Further improvement to the numerical results can be done by increasing the bond dimension of local tensors. This can increase the accuracy of the PEPS wave functions, especially for the low-energy excitation modes with long correlation

lengths, and improve the energy resolution of dynamical correlation functions. Increasing the bond dimension can be implemented either by taking a brute force calculation with a large-scale supercomputer or by imposing the symmetry of total spin along the z -axis. In our calculation, the wave function of the excitation mode is obtained by replacing just one local tensor from the ground state and then boosting it into a momentum eigenstate with the translation operator. If more local tensors are replaced, the accuracy of the result can be also improved.

Methods The tensor-network renormalization group methods [30, 31, 35–37] are used to calculate dynamical response functions of the anisotropic Heisenberg model, defined in Eq. (1), with $J = 1.67$ meV and $\Delta = 0.95$. A translation invariant PEPS on an infinite lattice is used to represent the ground state with 120° antiferromagnetic order. An ansatz based on the single-mode approximation [31, 35–37] is used to construct the wave functions of excitation states. The local tensors for both the ground state and the excitation states are optimized by minimizing the corresponding energies with the aid of automatic differentiation [30, 31]. Physical observables are obtained by contracting a double-layer PEPS formed from the initial and final states with the corner transfer matrix renormalization group [38–40]. The dynamical spectral functions shown in the text are obtained by expanding delta function with a Lorentzian broadening factor $\varepsilon = 0.04$ meV. Due to the heavy demand for the computational resources, both computational time and memory space, the largest bond dimension used in our calculation is 4 if the spectral functions on the whole momentum path are evaluated. For more technical details, please refer to SM.

Acknowledgements

We thank Tao Li, Chun Zhang, Yi-Bin Guo and Xuan Li for helpful discussions. We thank Hidekazu Tanaka for providing the reference data. This work is supported by the National Key Research and Development Project of China (Grant No. 2017YFA0302901), the National Natural Science Foundation of China (Grants Nos. 11888101, 11874095, and 11974396), the Youth Innovation Promotion Association CAS (Grants No. 2021004), and the Strategic Priority Research Program of Chinese Academy of Sciences (Grant Nos. XDB33010100 and XDB33020300).

-
- [1] P. Anderson, *Materials Research Bulletin* **8**, 153 (1973).
 - [2] L. Balents, *Nature* **464**, 199 (2010).
 - [3] H. J. Liao, Z. Y. Xie, J. Chen, Z. Y. Liu, H. D. Xie, R. Z. Huang, B. Normand, and T. Xiang, *Phys. Rev. Lett.* **118**, 137202 (2017).
 - [4] M. Mourigal, M. Enderle, A. Klöpperpieper, J.-S. Caux, A. Stunault, and H. M. Rønnow, *Nature Physics* **9**, 435 (2013).
 - [5] C. Castelnovo, R. Moessner, and S. L. Sondhi, *Nature* **451**, 42 (2008).
 - [6] P. Fazekas and P. W. Anderson, *Philosophical Magazine* **30**, 423 (1974).
 - [7] D. A. Huse and V. Elser, *Physical Review Letters* **60**, 2531 (1988).
 - [8] L. Capriotti, A. E. Trumper, and S. Sorella, *Phys. Rev. Lett.* **82**, 3899 (1999).
 - [9] S. R. White and A. L. Chernyshev, *Physical review letters* **99**, 127004 (2007).

- [10] J. Ma, Y. Kamiya, T. Hong, H. B. Cao, G. Ehlers, W. Tian, C. D. Batista, Z. L. Dun, H. D. Zhou, and M. Matsuda, *Phys. Rev. Lett.* **116**, 087201 (2016).
- [11] S. Ito, N. Kurita, H. Tanaka, S. Ohira-Kawamura, K. Nakajima, S. Itoh, K. Kuwahara, and K. Kakurai, *Nature Communications* **8**, 235 (2017).
- [12] D. Macdougall, S. Williams, D. Prabhakaran, R. I. Bewley, D. J. Voneshen, and R. Coldea, *Physical Review B* **102**, 064421 (2020).
- [13] T. Susuki, N. Kurita, T. Tanaka, H. Nojiri, A. Matsuo, K. Kindo, and H. Tanaka, *Physical Review Letters* **110**, 267201 (2013).
- [14] D. Yamamoto, G. Marmorini, and I. Danshita, *Physical Review Letters* **114**, 027201 (2015).
- [15] Y. Shirata, H. Tanaka, A. Matsuo, and K. Kindo, *Physical Review Letters* **108**, 057205 (2012).
- [16] G. Koutroulakis, T. Zhou, Y. Kamiya, J. D. Thompson, H. D. Zhou, C. D. Batista, and S. E. Brown, *Physical Review B* **91**, 024410 (2015).
- [17] W. Zheng, J. O. Fjaerestad, R. R. P. Singh, R. H. McKenzie, and R. Coldea, *arXiv* **74**, 224420 (2006).
- [18] O. A. Starykh, A. V. Chubukov, and A. G. Abanov, *Physical Review B* **74**, 180403 (2006).
- [19] A. L. Chernyshev and M. E. Zhitomirsky, *Physical Review B* **79**, 144416 (2009).
- [20] M. Mourigal, W. T. Fuhrman, A. L. Chernyshev, and M. E. Zhitomirsky, *Physical Review B* **88**, 094407 (2013).
- [21] R. Verresen, R. Moessner, and F. Pollmann, *Nature Physics* **15**, 750 (2019).
- [22] A. Mezio, C. N. Sposetti, L. O. Manuel, and A. E. Trumper, *EPL (Europhysics Letters)* **94**, 47001 (2011).
- [23] E. A. Ghioldi, A. Mezio, L. O. Manuel, R. R. P. Singh, J. Oitmaa, and A. E. Trumper, *Physical Review B* **91**, 134423 (2015).
- [24] E. A. Ghioldi, M. G. Gonzalez, S.-S. Zhang, Y. Kamiya, L. O. Manuel, A. E. Trumper, and C. D. Batista, *Phys. Rev. B* **98**, 184403 (2018).
- [25] S.-S. Zhang, E. A. Ghioldi, Y. Kamiya, L. O. Manuel, A. E. Trumper, and C. D. Batista, *Phys. Rev. B* **100**, 104431 (2019).
- [26] F. Ferrari and F. Becca, *Physical Review X* **9**, 031026 (2019).
- [27] C. Zhang and T. Li, *Physical Review B* **102**, 075108 (2020).
- [28] F. Verstraete and J. I. Cirac, [arXiv:cond-mat/0407066v1](https://arxiv.org/abs/cond-mat/0407066v1).
- [29] R. Orús, *Nature Reviews Physics* **1**, 538 (2019).
- [30] H.-J. Liao, J.-G. Liu, L. Wang, and T. Xiang, *Physical Review X* **9**, 31041 (2019).
- [31] B. Ponsioen, F. F. Assaad, and P. Corboz, *SciPost Phys.* **12**, 6 (2022).
- [32] Y. Doi, Y. Hinatsu, and K. Ohoyama, *Journal of Physics: Condensed Matter* **16**, 8923 (2004).
- [33] Y. Kamiya, L. Ge, T. Hong, Y. Qiu, D. L. Quintero-Castro, Z. Lu, H. B. Cao, M. Matsuda, E. S. Choi, C. D. Batista, M. Mourigal, H. D. Zhou, and J. Ma, *Nature communications* **9**, 2666 (2018).
- [34] R. P. Feynman, *Phys. Rev.* **94**, 262 (1954).
- [35] S. Östlund and S. Rommer, *Phys. Rev. Lett.* **75**, 3537 (1995).
- [36] J. Haegeman, B. Pirvu, D. J. Weir, J. I. Cirac, T. J. Osborne, H. Verschelde, and F. Verstraete, *Phys. Rev. B* **85**, 100408 (2012).
- [37] L. Vanderstraeten, M. Mariën, F. Verstraete, and J. Haegeman, *Physical Review B* **92**, 201111 (2015).
- [38] T. Nishino and K. Okunishi, *Journal of the Physical Society of Japan* **65**, 891 (1996).
- [39] R. Orús and G. Vidal, *Phys. Rev. B* **80**, 094403 (2009).
- [40] P. Corboz, T. M. Rice, and M. Troyer, *Phys. Rev. Lett.* **113**, 046402 (2014).

Supplementary material

Spin excitation spectra of the spin-1/2 triangular Heisenberg antiferromagnets from tensor networks

Run-Ze Chi,^{1,2,*} Yang Liu,^{1,2,*} Yuan Wan,^{1,3} Hai-Jun Liao,^{1,3,†} and T. Xiang^{1,2,4,‡}

¹Beijing National Laboratory for Condensed Matter Physics and Institute of Physics, Chinese Academy of Sciences, Beijing 100190, China.

²School of Physical Sciences, University of Chinese Academy of Sciences, Beijing 100049, China.

³Songshan Lake Materials Laboratory, Dongguan, Guangdong 523808, China.

⁴Beijing Academy of Quantum Information Sciences, Beijing, China.

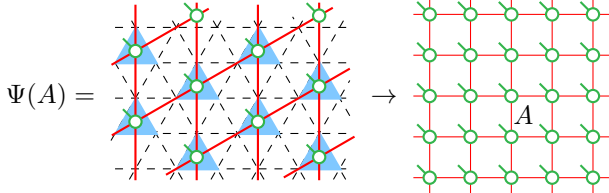
I. CALCULATION OF THE EXCITATION STATES

To simulate the magnetic excitations of $\text{Ba}_3\text{CoSb}_2\text{O}_9$, we need to calculate the zero-temperature dynamical spectral function

$$\begin{aligned} S^{\alpha\beta}(\mathbf{k}, \omega) &= \langle 0 | S_{-\mathbf{k}}^\alpha \delta(\omega - H + E_0) S_{\mathbf{k}}^\beta | 0 \rangle \\ &= \sum_m \langle 0 | S_{-\mathbf{k}}^\alpha | m \rangle \langle m | S_{\mathbf{k}}^\beta | 0 \rangle \delta(\omega - E_m + E_0), \end{aligned} \quad (\text{S1})$$

where H is the Hamiltonian, $\alpha, \beta = x, y, z$ are the spin components. $|0\rangle$ and $|m\rangle$ are the ground state and excited states, respectively. E_0 and E_m are the corresponding energy eigenvalues.

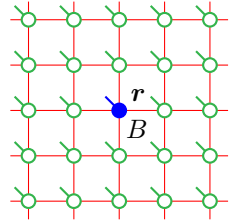
In our calculation, the ground state $|0\rangle \equiv |\Psi(A)\rangle$ is represented as an infinite projected entangled-pair state (iPEPS) on a deformed square lattice, which is obtained from the original triangular lattice by grouping three sites on a triangle into just one site



Local tensor A is assumed to be translation invariant. It contains three physical spins and is determined by variationally minimizing the ground state energy. This minimization can be readily implemented by making use of the approach of automatic differentiation [S1]. An accurate determination of local tensor A is crucial to the accurate calculation of the excited states.

In the framework of tensor-network states, each excited state $|m\rangle$ is well described by a superposed wave function of all locally perturbed states on top of the ground state constructed based on the single-mode approximation [S2]. More specifically, $|m\rangle$ is obtained in two steps: First, we replace the

local tensor A at site \mathbf{r} in $|\Psi(A)\rangle$ with a new tensor B and denote the resulting state as $|\Phi_{\mathbf{r}}(B)\rangle$,



$$\Phi_{\mathbf{r}}(B) = \quad (\text{S2})$$

Second, we boost $|\Phi_{\mathbf{r}}(B)\rangle$ into a momentum eigenstate using the translation operator and denote it as

$$|\Phi_{\mathbf{k}}(B)\rangle = \sum_{\mathbf{r}} e^{i\mathbf{k}\cdot\mathbf{r}} |\Phi_{\mathbf{r}}(B)\rangle \quad (\text{S3})$$

where $|\Phi_{\mathbf{k}}(B)\rangle$ is a superposition of all perturbed states $|\Phi_{\mathbf{r}}(B)\rangle$ with appropriate phase factors. This single-mode approximated wave function was first introduced in the framework of matrix product states (MPS) by Ostlund and Rommer in one dimension [S3, S4]. It was extended to PEPS in two dimensions by Vanderstraeten *et al.* [S5].

The excited states should be orthogonal to the ground state. This requires that the perturbed state $|\Phi_{\mathbf{r}}(B)\rangle$ is a vector in the tangent space of the ground state, satisfying the constraint

$$\langle \Phi_{\mathbf{r}}(B^\dagger) | \Psi(A) \rangle = 0. \quad (\text{S4})$$

As the dimension of local tensor A is dD^4 , the dimension of the tangent space is at most $M = dD^4 - 1$, where D is the virtual bond dimension of A and $d = 8$ is the dimension of the physical index. This implies that there are at most M linearly independent vectors B_m in the tangent space.

To find the excited states, we start from M linearly independent of vectors $\{\tilde{B}_m, m = 1, \dots, M\}$ in the tangent space of the ground state. The momentum eigenstates constructed from these local \tilde{B} -tensors are also linearly independent, but they are usually not orthogonal to each other

$$N_{mn}^{\text{eff}} = \langle \Phi_{\mathbf{k}}(\tilde{B}_m^\dagger) | \Phi_{\mathbf{k}}(\tilde{B}_n) \rangle. \quad (\text{S5})$$

Within this set of basis states, the Hamiltonian are effectively described by the matrix elements

$$H_{mn}^{\text{eff}} = \langle \Phi_{\mathbf{k}}(\tilde{B}_m^\dagger) | H | \Phi_{\mathbf{k}}(\tilde{B}_n) \rangle. \quad (\text{S6})$$

* These authors contributed equally to this work

† navyphysics@iphy.ac.cn

‡ txiang@iphy.ac.cn

Since H_{mn}^{eff} is a linear function of local tensor \tilde{B}_m^\dagger and \tilde{B}_n , it can be also written as

$$H_{mn}^{\text{eff}} = \tilde{B}_m^\dagger \mathbb{H}_k \tilde{B}_n, \quad (\text{S7})$$

where \mathbb{H}_k is a $M \times M$ matrix. As \mathbb{H}_k does not explicitly depend on \tilde{B} -tensors, the above expression suggests that $\mathbb{H}_k \tilde{B}_n$ can be determined by simply taking the derivative of the diagonal term of the effective Hamiltonian H_{nn}^{eff} with respect to \tilde{B}_n^\dagger , namely,

$$\left(\mathbb{H}_k \tilde{B}_n \right) = \frac{\partial}{\partial \tilde{B}_n^\dagger} \left(\tilde{B}_n^\dagger \mathbb{H}_k \tilde{B}_n \right). \quad (\text{S8})$$

This derivative, as discussed in Ref. [S6], can be implemented using automatic differentiation [S1]. From this derivative, we can obtain all the matrix elements of H_{mn}^{eff} , namely,

$$H_{mn}^{\text{eff}} = \tilde{B}_m^\dagger \left(\mathbb{H}_k \tilde{B}_n \right), \quad m = 1, \dots, M. \quad (\text{S9})$$

By solving the following generalized eigen-equation,

$$\sum_n H_{mn}^{\text{eff}} v_{np} = \sum_n \omega_p N_{mn}^{\text{eff}} v_{np}. \quad (\text{S10})$$

we eventually obtain the B -tensor of the p -th excited state

$$B_p = \sum_n \tilde{B}_n v_{np}, \quad (\text{S11})$$

and the corresponding excitation energy ω_p .

The major computational cost is to evaluate the derivative of H_{nn}^{eff} for each independent excited basis state, which scales as $O(D^{12})$ [S1, S6]. For each given momentum point \mathbf{k} , as there are M excited basis states, the total computational cost scales as $O(dD^4 \times D^{12}) \sim O(dD^{16})$.

II. SUM RULE OF THE DYNAMICAL SPECTRAL FUNCTION

After obtaining the wave functions of the excitation states, we can calculate the dynamical spectral function using the formula

$$S^{\alpha\alpha}(\mathbf{k}, \omega) = \sum_m w_{\mathbf{k}}^\alpha(m) \delta(\omega - E_m + E_0), \quad (\text{S12})$$

where

$$w_{\mathbf{k}}^\alpha(m) = \left| \langle \Phi_{\mathbf{k}}(B_m^\dagger) | S_{\mathbf{k}}^\alpha | \Psi(A) \rangle \right|^2 \quad (\text{S13})$$

is the spectral weight. If the single-spin excited states $|\Phi_{\mathbf{k}}(B_m)\rangle$ are complete, it is expected that the dynamical spectral function should satisfy the following sum rule

$$\sum_{m\alpha} w_{\mathbf{k}}^\alpha(m) = \sum_{\alpha} \left[\langle \Psi(A) | S_{-\mathbf{k}}^\alpha S_{\mathbf{k}}^\alpha | \Psi(A) \rangle - \left| \langle \Psi(A) | S_{\mathbf{k}}^\alpha | \Psi(A) \rangle \right|^2 \right]. \quad (\text{S14})$$

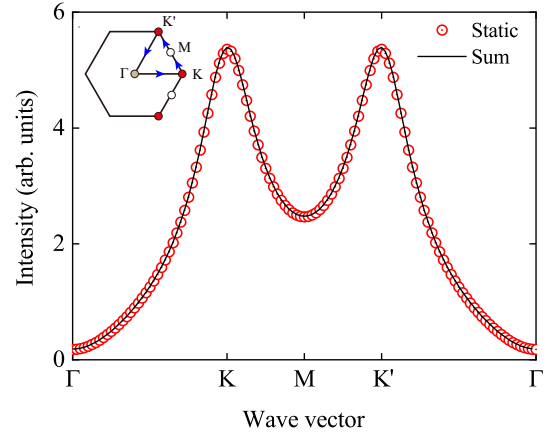


FIG. S1. **Verification of the sum rule for the dynamical spectral function.** Comparison of the total spectral weights (black curve) with the static spin structure factor (red circles) along the momentum path $\Gamma - K - M - K' - \Gamma$.

The right hand side of this equation is the static spin structure factor, which is determined purely by the ground state wave function.

Fig. S1 compares the total spectral weights with the static spin structure factor along the momentum path $\Gamma - K - M - K' - \Gamma$. Apparently, the sum rule is satisfied. It implies that the single-mode PEPS wave functions provide a complete description of all single-spin excitation states.

III. BOND DIMENSION DEPENDENCE OF THE MINIMAL EXCITATION ENERGY GAP

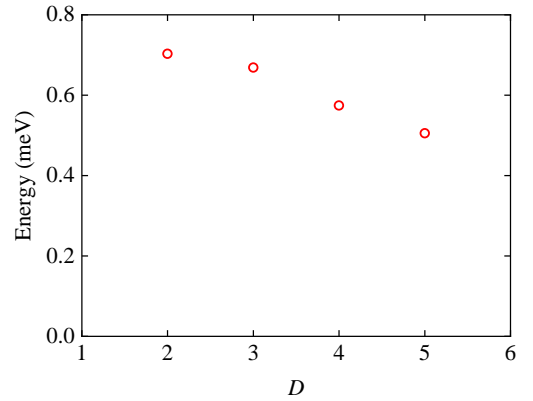


FIG. S2. **Minimal spectral gap as a function of bond dimension D .** The lowest spectral gap of the XXZ model occurs at the K point (see. Fig. S1) in the Brillouin zone. The gap values are obtained by contracting the effective Hamiltonian tensor network states of the excited states using the corner transfer matrix renormalization group method with a bond dimension $\chi = 50$ for $D = 2, 3, 4$ and $\chi = 60$ for $D = 5$.

The ground state of the XXZ model we studied is 120° Néel ordered. It breaks the planar $U(1)$ continuous symmetry of

the XXZ model and should have a gapless excitation mode according to the Goldstone theorem. However, in the PEPS representations of the ground state with a finite bond dimension D , the excitation is always gapped. The gap becomes zero only in the limit $D \rightarrow \infty$. At any finite D , it is expected that the minimal excitation gap should decrease with the increase of D . This, as shown in Fig. S2, is indeed what we see

in our calculation.

In principle, the energy gap should converge with D in certain power law for sufficiently large D in a gapless system [S7]. As the values of D that were used in our calculation are still very small, our data have not yet entered this power-law converged regime.

-
- [S1] H.-J. Liao, J.-G. Liu, L. Wang, and T. Xiang, *Physical Review X* **9**, 31041 (2019).
- [S2] R. P. Feynman, *Phys. Rev.* **94**, 262 (1954).
- [S3] S. Östlund and S. Rommer, *Phys. Rev. Lett.* **75**, 3537 (1995).
- [S4] J. Haegeman, B. Pirvu, D. J. Weir, J. I. Cirac, T. J. Osborne, H. Verschelde, and F. Verstraete, *Phys. Rev. B* **85**, 100408 (2012).
- [S5] L. Vanderstraeten, M. Marin, F. Verstraete, and J. Haegeman, *Physical Review B* **92**, 201111 (2015).
- [S6] B. Ponsioen, F. F. Assaad, and P. Corboz, *SciPost Phys.* **12**, 6 (2022).
- [S7] H. J. Liao, Z. Y. Xie, J. Chen, Z. Y. Liu, H. D. Xie, R. Z. Huang, B. Normand, and T. Xiang, *Phys. Rev. Lett.* **118**, 137202 (2017).